Article:
Lishchuk, SV and Ettelaie, R (2020) Detachment work of prolate spheroidal particles from fluid droplets: role of viscous dissipation. Soft Matter. C9SM02385. ISSN: 1744-683X

https://doi.org/10.1039/c9sm02385b

Soft Matter

Accepted Manuscript

This article can be cited before page numbers have been issued, to do this please use: S. V. Lishchuk and R. Ettelaie, *Soft Matter*, 2020, DOI: 10.1039/C9SM02385B.

ROYAL SOCIETY OF CHEMISTRY

rsc.li/soft-matter-journal

View Article Online
DOI: 10.1039/C9SM02385B

Detachment work of prolate spheroidal particles from fluid droplets: role of viscous dissipation

Sergey V. Lishchuk[1] and Rammile Ettelaie[2]

[1] *Materials and Engineering Research Institute, Sheffield Hallam University, Sheffield S1 1WB, UK*
[2] *Food Colloids Group, School of Food Science and Nutrition, University of Leeds, Leeds LS2 9JT, UK*

The force–displacement curve for removal of an elongated solid particle from the surface of liquid droplets or gas bubbles is calculated and compared to our previous reported results for spherical particles. The surface adsorption energy for prolate particles is known to be larger than those of spheres. We show that in fact the minimum possible work done upon removal of an elongated particle from surface can be less than that for a sphere. This result is obtained when the dissipation of interfacial energy, stored in the fluid film, attaching the particles to the surface during their displacement, is properly accounted for. This dissipation is unavoidable, even if the particles are removed infinitely slowly. Once the particle actually leaves the surface, the formed liquid bridge relaxes thus dissipating any stored interfacial energy as the surface returns to its original undistorted state. The difference between the work of removal of a particle from surface and its adsorption energy is seen to become increasingly larger with smaller particle to droplet size ratios. For example, for a size ratio of 1:100, the work of removal is 1.93 times greater than the adsorption energy. However, we also find that for any given size ratio, there is a value of particle aspect ratio for which the work of removal of particles (combined dissipated and adsorbed energy) attains its minimum value.

I. INTRODUCTION

Fluid interfaces laden with elongated particles have a number of distinct properties. Anisotropy in capillary [1–10] and fluctuation-induced [2, 11] interactions between ellipsoidal particles leads to self-assembled structures otherwise not observed for spherical particles [12–16]. These also lead to stronger surface rheological response [14]. As a result, ellipsoidal particles are very efficient in stabilising emulsions [17, 18]. Ellipsoidal particles demonstrate the enhanced translation drag [19], stronger sensitivity of the contact angle to surface chemical and topographical heterogeneities [20], and an ability to suppress coffee ring effect [21, 22]. The fluid interfaces laden with Janus ellipsoidal particles is exhibit an even richer diversity of behaviours [23, 24].

In the absence of line tension, it is energetically favourable for ellipsoids to be oriented parallel to the interface to maximise the amount of displaced area of the fluid interface [2]. However, particles may take other orientations in order to reduce the contribution of line tension to the free energy [25], or to adapt to the external applied electric or magnetic fields [26, 27], or indeed to relieve the compressional stress [17, 28]. During the adsorption process, ellipsoidal particles dynamically take different orientations before reaching the stable orientation [29–31]. In membrane biology, flipping of the ellipsoidal shaped proteins may be responsible for suppressing transmembrane proton transfer [32].

Faraudo and Bresme [25] found that, due to line tension, elongated particles can more easily be removed from the fluid interface when compared to the spherical ones. Line tension can affect the behaviour of the adsorbed particles if the particles are small enough [33–35], and thus can be relevant to nanoparticles. For larger particles, when the contribution of line tension to the free energy is negligible, Davies et al. [36] developed a detachment energy model for spheroids based on free energy difference between the particle at the interface and the ones in the bulk. The authors have concluded that prolate and oblate spheroidal particles attach to interfaces more strongly because they reduce the interface area more than spherical particles for a given particle volume.

Our work [37] revealed increasing role of post-detachment dissipation of energy with increasing droplet-to-particle size ratio in relation to the detachment work. This indicated the existence of a significantly higher energy barrier to desorption of very small particles, compared to the value suggested purely based on their adsorption energy alone. Here we investigate the effect of viscous energy dissipation in detachment of a spheroidal particle from a fluid droplet. We investigate how the account of energy dissipation may qualitatively change the behaviour of the minimum detachment work with the aspect ratio of particles.

II. MODEL

We consider the detachment process as shown in Figure 1. Stage I is the rotation of the particle from the minimum energy state to the vertical orientation. In stage II the force is applied to the particle to displace it from the equilibrium position until detachment. In stage III the fluid interface relaxes to its equilibrium position. If stages I and II are slow enough then there is no dissipation, and the work done equals the free energy difference. However, energy dissipation in stage III, which occurs due to fluid flow, is unavoidable. This is due to the relaxation of the liquid bridge, and the dissipation of the interfacial energy stored in it, once the particle leaves the surface. We argue that the process shown in Figure 1 in the slow

View Article Online
DOI: 10.1039/C9SM02385B

limit requires minimum work.

In order to calculate the work of detachment, we consider the geometry shown in Figure 2. Two spheroidal particles with three semi-axes a, a and Aa, where A is the aspect ratio, are located at the opposite ends of the droplet. This geometry is similar to the one used in our previous studies [37, 38].

III. FORCE–DISPLACEMENT DIAGRAM

In order to facilitate analytical calculation, we consider the limit of small ratio of particle to drop sizes,

$$\nu \equiv \frac{a}{R} \ll 1, \tag{1}$$

where R is the radius of the droplet. The analysis proceeds in a similar manner to the case of spherical particles [37] with the appropriate modifications made due to spheroidal shape. The derivation presented in the Appendix yields the analytical expression for the dependence between the force F and the displacement Δr of the particles from their equilibrium positions in the absence of any applied force. This dependence can be represented in a parametrical form as

$$F(\kappa) = \pi\gamma a\mu \tag{2}$$

and

$$\Delta r(\kappa) = a\left\{A\sqrt{1-\kappa^2} - \frac{\mu}{4}\left[1 + 2\ln\frac{(\kappa+\xi)\nu}{4}\right]\right\}, \tag{3}$$

where in these formulas

$$\xi = \sqrt{\kappa^2 - \frac{\mu^2}{4}}, \tag{4}$$

$$\mu = \frac{2\kappa\left(\sqrt{1-\kappa^2}\sin\theta - A\kappa\cos\theta\right)}{\sqrt{1+(A^2-1)\kappa^2}}, \tag{5}$$

θ is the contact angle between the fluid interface and the surface of the particle, and γ is the interfacial tension between the droplet and its surrounding medium. The parameter κ changes between $\kappa_{\min}$ and $\kappa_{\max}$, where $\kappa_{\min}$ is the solution of the equation

$$\left.\frac{d\Delta r(\kappa)}{d\kappa}\right|_{\kappa=\kappa_{\min}} = 0, \tag{6}$$

and $\kappa_{\max}$, the dimensionless radius of the contact line in absence of the external force, is given by formula

$$\kappa_{\max} = \frac{\sin\theta}{\sqrt{1+(A^2-1)\cos^2\theta}}. \tag{7}$$

At the values of the aspect ratio $A = 0$ and $A = 1$ these formulas reduce to the cases of spherical particles with pinned [38] and free [37] contact lines, respectively. The force–displacement dependence for different values of A and ν is illustrated in Figure 3 and Figure 4, in which the small radius of the particle, a, is being kept constant.

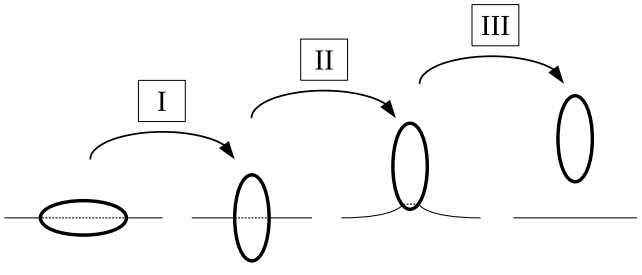

FIG. 1. Sketch of detachment process with the lowest amount of minimum work.

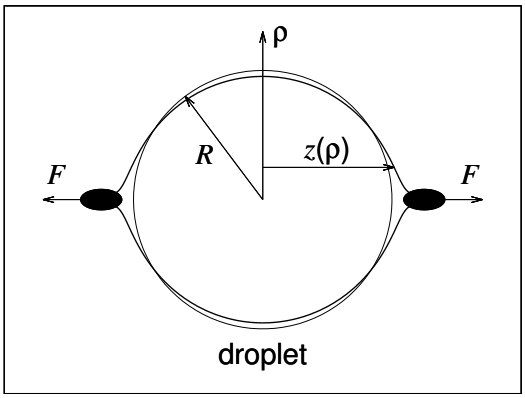

(a)

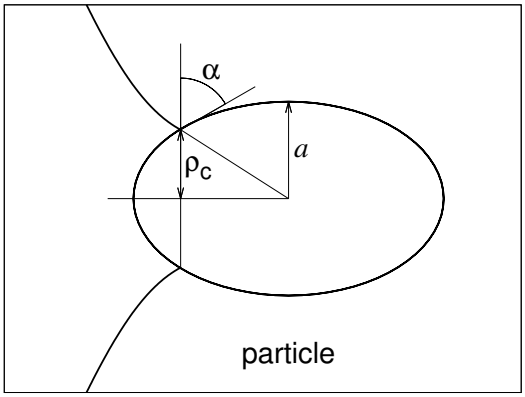

(b)

FIG. 2. Geometry of the system considered in this work: (a) two particles placed at the opposite ends of the droplet, and (b) the liquid bridge formed during displacement of a particle from the surface.

View Article Online
DOI: 10.1039/C9SM02385B

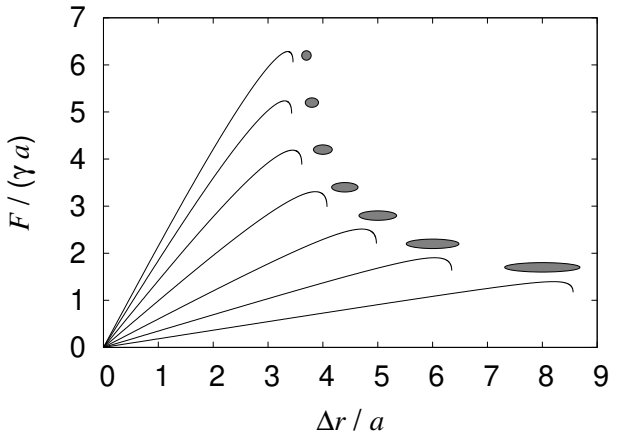

FIG. 3. Dependence of force upon the position of the particles at $\theta = 90^\circ$, $\nu = 0.01$, and $A = 1, 1.4, 2, 2.8, 4, 5.6, 8$ (from top to bottom).

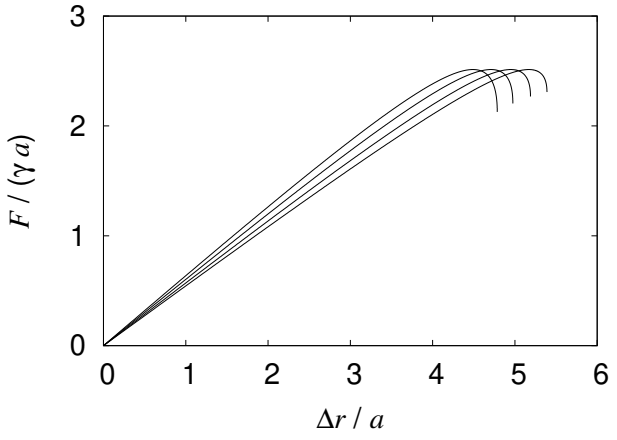

FIG. 4. Dependence of force upon the position of the particles at $\theta = 90^\circ$, $A = 4$, and $\nu = 0.03, 0.01, 0.003, 0.001$ (from left to right).

IV. MINIMUM WORK OF DETACHMENT

In order to simplify further analysis, we consider the special case of right contact angle ($\theta = 90^\circ$). This allows us to determine that the maximum force, which is given by formula

$$F^* = \frac{2\pi\gamma a}{A+1} \tag{8}$$

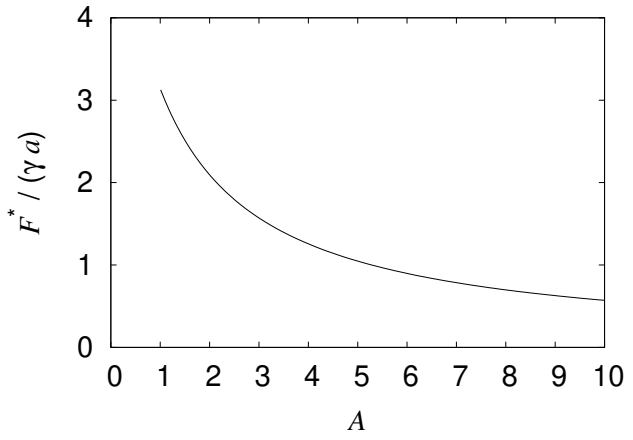

FIG. 5. Dependence of the detachment force upon A, when the contact angle $\theta = 90^\circ$.

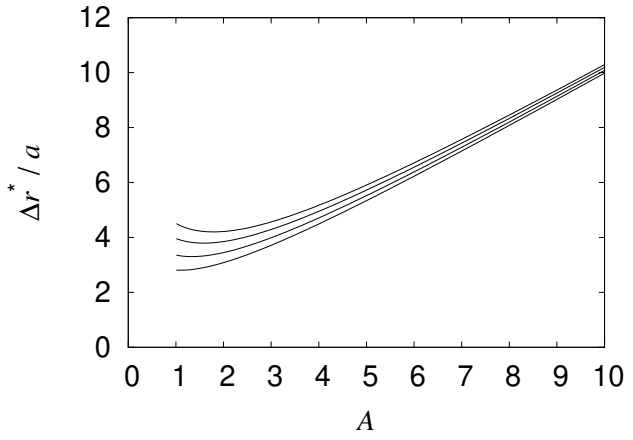

FIG. 6. Dependence of particle displacement at a point of maximum force upon A for $\theta = 90^\circ$ and $\nu = 0.03, 0.01, 0.003, 0.001$ (from bottom to top).

which is plotted in Figure 5 as a function of A, and occurs at a particle displacement of

$$\Delta r^* = -\frac{a}{A+1} \times \times \left[\ln \frac{\left(\sqrt{A} + \sqrt{A+1}\right)\nu}{4(A+1)} - A^{3/2}\sqrt{A+1} + \frac{1}{2} \right]. \tag{9}$$

The value of Δr^*, the displacement at which the maximum force occurs before the particle is detached from the surface, is plotted against A in Figure 6. The force-displacement curves are linear for small displacements, with a clear deviation from the linear behaviour occurring at displacements close to the point of detachment.

View Article Online
DOI: 10.1039/C9SM02385B 4

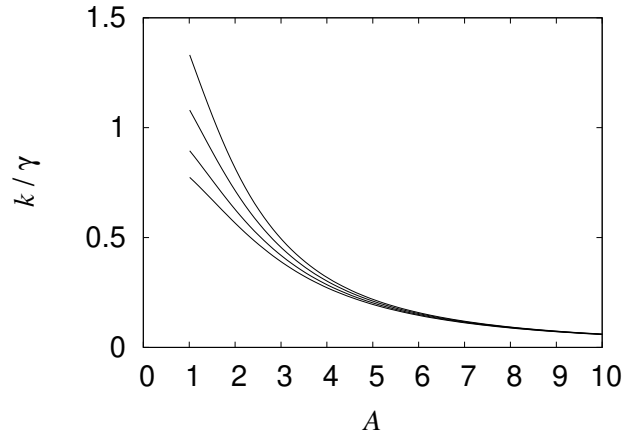

FIG. 7. Dependence of the Hooke–de Gennes constant upon A for $\theta = 90^\circ$ and $\nu = 0.03, 0.01, 0.003, 0.001$ (from top to bottom).

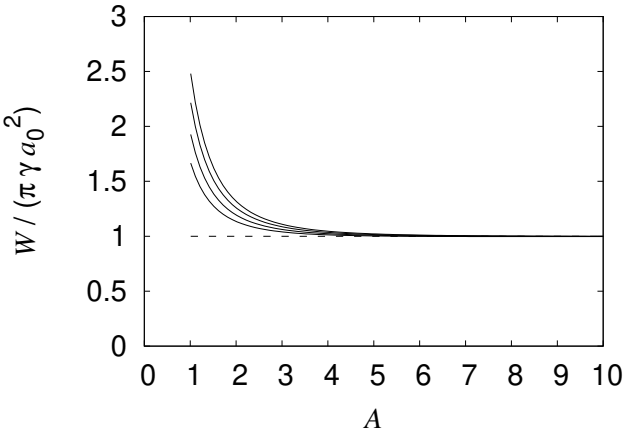

FIG. 8. Dependence of the detachment work upon A for $\theta = 90^\circ$ and $\nu_0 = 0.03, 0.01, 0.003, 0.001$ (from bottom to top). The coverage area is fixed. The dashed line shows the adsorption energy.

The so called Hooke–de Gennes constant, defined as

$$k = \left(\frac{dF}{d\Delta r}\right)_{\Delta r=0}, \tag{10}$$

is given by formula

$$k = \frac{2\pi\gamma}{A^2 - \frac{1}{2} - \ln\frac{\nu}{2}}. \tag{11}$$

and is plotted in Figure 7. The above formulas also reduce at $A = 0$ and $A = 1$ to the cases of spherical particles with pinned [38] and free [37] contact line, respectively.

We compare the detachment work at different particle elongations in two ways. First, we fix the fluid interface area covered by a particle at equilibrium. We choose this area to equal that taken by a spherical particle of radius a_0. In this case we have $a = A^{-1/2}a_0$ and $\nu = A^{-1/2}\nu_0$, where $\nu_0 \equiv a_0/R$. The detachment work for the stage II is then calculated by numerical integration of the force–displacement diagram,

$$W_{\mathrm{II}} = -\int_{\kappa_{\min}}^{1} F(\kappa)\frac{d\Delta r(\kappa)}{d\kappa}d\kappa, \tag{12}$$

where $F(\kappa)$ and $d\Delta r(\kappa)$ are given by Eqs (2) and (3), respectively, and $\kappa_{\min}$ is the solution of the equation (6). Note that the exact work required to remove the particle from the surface, and in particular the dissipated component of it, are path dependent. The value correspondent to the situation depicted in Figure 1 represents the minimum possible value for this quantity and serves as a lower limit for W.

As ν decreases, the dependence of the force upon the displacement of the particles becomes more linear. This allows us to obtain an approximate analytic expression for the detachment work at stage II in small particle to droplet size ratio limit, as being the area of the triangle on the force–displacement diagram:

$$W_{\mathrm{II}} = \frac{1}{2}k\left(\Delta r^*\right)^2, \tag{13}$$

where Hooke–de Gennes constant, k, and particle displacement corresponding to maximum force, Δr^*, are given by formulas (11) and (9), respectively. This work should be augmented by energy increase due to particle rotation in stage I,

$$W_{\mathrm{I}} = \pi\gamma a^2(A-1). \tag{14}$$

The total minimum work of detachment at $\theta = 90^\circ$ thus equals

$$W = W_{\mathrm{I}} + W_{\mathrm{II}} = \pi\gamma a^2\left\{A - 1 + \right. \tag{15}$$
$$\left. + \frac{\left[\ln\frac{\left(\sqrt{A}+\sqrt{A+1}\right)\nu}{4(A+1)} - A^{3/2}\sqrt{A+1} + \frac{1}{2}\right]^2}{(A+1)^2\left(A^2 - \frac{1}{2} - \ln\frac{\nu}{2}\right)}\right\}.$$

The dependence of the total detachment work $W = W_{\mathrm{I}} + W_{\mathrm{II}}$ upon the aspect ratio A at fixed area is depicted in Figure 8 and shows that with increasing elongation of particles the work of pulling out the particle quickly decreases compared to the work required to rotate the particle in the initial stage (stage I).

Instead of fixing the coverage area, we can also consider the case of a fixed particle volume. For a fixed volume of the particle we have $a = A^{-1/3}a_0$ and $\nu = A^{-1/3}\nu_0$. This case was considered by Davies et al. [36], who suggested that prolate and oblate spheroidal particles attach to interfaces more strongly. However, if we take into account the energy dissipation, this conclusion changes, and the

View Article Online
DOI: 10.1039/C9SM02385B

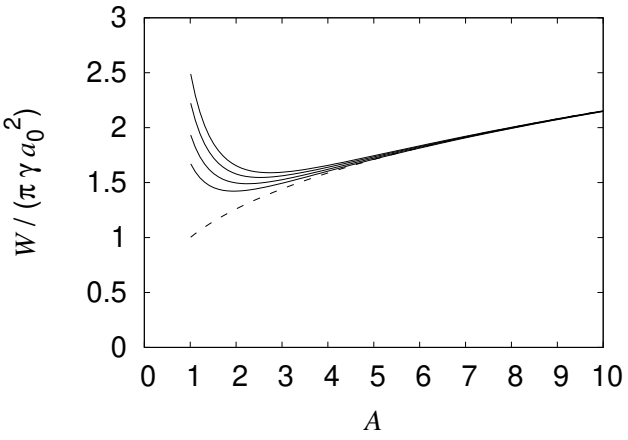

FIG. 9. Dependence of the detachment work upon A for a contact angle $\theta = 90^\circ$ and $\nu_0 = 0.03, 0.01, 0.003, 0.001$ (from bottom to top). The particle volume is fixed. The dashed line shows the adsorption energy, not accounting for any energy dissipation.

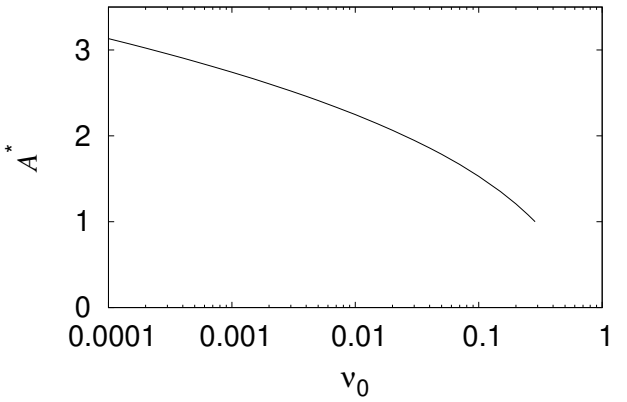

FIG. 10. Dependence upon ν_0 of the aspect ratio A^* for which the detachment work at fixed particle volume is minimal at $\theta = 90^\circ$.

detachment work takes its minimum value at an aspect ratio $A^* > 1$, as shown in Figure 9 and Figure 10.

Oblate spheroids are not considered in the present work because in this case the process with minimum detachment work involves anisotropic configurations which are difficult to analyse analytically.

V. CONCLUSION

We have considered deformation of a spherical droplet or a bubble containing a pair of prolate spheroidal particles on its surface in the case when equal but opposite forces are applied to the particles. The force-displacement curves, calculated as the particles are pulled apart, are found to be linear for small displacements. The deviation from the linear force–displacement behaviour occurs close to the point of detachment.

We have investigated the effect of viscous dissipation of energy upon the minimum detachment work for different aspect ratios of the particles. Even in an idealised situation such a dissipation occurs as a liquid bridge connecting the particle to the surface relaxes, once the particle has left the interface. Any stored energy in the liquid bridge from the distortion of the interface has to be dissipated as a result. We have found that, even in the absence of line tension, it is easier to remove elongated particles from fluid interfaces than spheres because of a smaller degree of this viscous dissipation of stored interfacial energy.

The force–displacement relationship obtained in this work can be directly verified in the experiments carried out with a spheroidal particle attached to a beam or cantilever [39, 40]. The complete detachment process sketched in Figure 1 can be realised, for example, by using magnetic particles for which both reorientation [26, 27] and detachment [41] in the external magnetic field can be controlled.

In the more common case of a fluid interface subjected to flow, it is more problematic to realise the process of detachment of the adsorbed particle with minimum work, as calculated here. This is because the forces acting on a particle favour different pathways [42] or result in a very fast process in which the energy dissipated even before the breaking of the liquid bridge cannot be neglected [43]. Investigation of the detailed detachment dynamics in each system and flow type is necessary to determine how different the detachment work from its minimum possible value will turn out to be.

If the particles or droplets are too large or too small, the model we presented should be modified by taking account of possible new physics. If the size of the droplet R is not small compared to the capillary length $\lambda_c = \sqrt{\gamma/\rho g}$ (g is the gravitational acceleration, ρ is the density of the fluid) then gravity force should also be taken into account. Conversely, in the case of small, nanometre sized particles a number of new effects can come into play. Line tension τ, already mentioned in Introduction, becomes important for particle sizes comparable to τ/γ [33–35]. This modifies the contact angle between nanoparticle and fluid interface [35, 44, 45]. The significance of the roughness and porosity of the particles upon the contact angle also increases with decreasing size of the particle [44]. At very small particle sizes the effects of thermal fluctuations may become noticeable [46].

Another modification of the model would be required at the nanoscale in the case when there is a surfactant film adsorbed at the interface. In this case there is an additional contribution to the surface free energy due to deformation of the surfactant-laden fluid interface [47]. This contribution is important when the radius of curvature of the interface becomes comparable with $\sqrt{\kappa/\gamma}$,

View Article Online
DOI: 10.1039/C9SM02385B 6

where κ is the bending rigidity of the interface. Such curvatures are expected for nanometre-sized particles.

CONFLICTS OF INTEREST

There are no conflicts to declare.

Appendix: Derivation of force–displacement relation

This Appendix presents the derivation of the parametrical dependence between the force F and the displacement Δr of the particles in the small-particle limit $\nu \ll 1$. The derivation closely follows the case of the spherical particles, described in detail in Ref. [37], but with modifications made to account for the spheroidal shape of the particles.

The axially symmetric shape of the droplet at arbitrary outward displacement of the particles is unduloid, which can be described in cylindrical polar coordinates (ρ, z) by formula [37]

$$z = \rho_+ E(\varphi, k) + \frac{c\rho_0}{2\rho_+} F(\varphi, k). \tag{A.1}$$

Here $F(\varphi, k)$ and $\mathrm{E}(\varphi, k)$ are incomplete elliptic integrals of first and second kind, respectively, where we have defined

$$\sin\varphi = \sqrt{\frac{\rho_+^2 - \rho^2}{\rho_+^2 - \rho_-^2}}, \tag{A.2}$$

$$k = \sqrt{1 - \frac{\rho_-^2}{\rho_+^2}}, \tag{A.3}$$

$$\rho_\pm = \sqrt{\frac{1 - c \pm \sqrt{1 - 2c}}{2}}\rho_0. \tag{A.4}$$

The constants ρ_0 and c arise from the solution of the second-order Euler-Lagrange differential equation, which corresponds to the variational problem of minimisation of the area of the droplet surface, and are determined by the boundary conditions at the particle-droplet interface and the condition of incompressibility of the droplet [37]. The derivative of the function $z(\rho)$ is expressed in elementary functions as

$$z' = -\frac{\frac{1}{2}c\rho_0^2 + \rho^2}{\sqrt{\rho_0^2\rho^2 - \left(\frac{1}{2}c\rho_0^2 + \rho^2\right)^2}} \tag{A.5}$$

Incompressibility of the droplet implies conservation of droplet volume which, in turn, is given by formula

$$\begin{aligned} V = \frac{4\pi}{3}\Bigg\{ &\left[\left(1 - \frac{c}{4}\right)\rho_0^2 - \frac{3}{2}\rho_c^2\right]\rho_+ E(\varphi_c, k) \\ &- \left[\frac{\rho_-^2\rho_+}{2} + \frac{3}{4}\frac{c\rho_0^2\rho_c^2}{\rho_+}\right] F(\varphi_c, k) \\ &+ \frac{\rho_c}{2}\sqrt{\left(\rho_+^2 - \rho_c^2\right)\left(\rho_c^2 - \rho_-^2\right)} \\ &+ \frac{3}{2}\rho_c^2 r - A\left[a^3 - \left(a^2 - \rho_c^2\right)^{3/2}\right]\Bigg\}, \end{aligned} \tag{A.6}$$

where the contact radius ρ_c is defined as shown in Figure 2. This formula explicitly includes the aspect ratio of the spheroidal particles to account for protrusion of particles into the droplet and therefore the region of the droplet that is occupied by a part of the particle.

To obtain the explicit formula for the free energy of the system, we need the expressions for the contact areas between different constituent phases. Integrating the surface area of the spheroid perturbing out of the droplet, we can represent the interfacial areas of a spheroidal particle in contact with fluids 1 and 2 as

$$\begin{aligned} S_{1p} = 2\pi a^2 \Bigg[&1 + \frac{A^2}{\sqrt{A^2 - 1}} \arcsin\frac{\sqrt{A^2 - 1}}{A^2} \\ &- \sqrt{1 - \kappa^2}\sqrt{1 + (A^2 - 1)\kappa^2} \\ &- \frac{A^2}{\sqrt{A^2 - 1}} \arcsin\frac{\sqrt{1 - \kappa^2}\sqrt{A^2 - 1}}{A^2}\Bigg] \end{aligned} \tag{A.7}$$

and

$$\begin{aligned} S_{2p} = 2\pi a^2 \Bigg[&1 + \frac{A^2}{\sqrt{A^2 - 1}} \arcsin\frac{\sqrt{A^2 - 1}}{A^2} \\ &+ \sqrt{1 - \kappa^2}\sqrt{1 + (A^2 - 1)\kappa^2} \\ &+ \frac{A^2}{\sqrt{A^2 - 1}} \arcsin\frac{\sqrt{1 - \kappa^2}\sqrt{A^2 - 1}}{A^2}\Bigg], \end{aligned} \tag{A.8}$$

where

$$\kappa \equiv \frac{\rho_c}{a}. \tag{A.9}$$

As the particles are displaced from their equilibrium positions, the radius of the contact line, ρ_c, made at the contact between the solid and the fluid media 1 and 2, alters and therefore also κ. As a result, the free energy of the system, up to a constant additive term, is

$$\mathcal{F} = \gamma_{1p}S_{1p} + \gamma_{2p}S_{2p} + \gamma S_{12}, \tag{A.10}$$

where γ_{1p} and γ_{2p} are surface tensions of the surface of the particles in contact with fluids 1 and 2, respectively. This leads to

$$\mathcal{F} = 4\pi\gamma\left[\rho_+\rho_0 E(\varphi_c, k) - \frac{a^2}{2}B(\kappa)\cos\theta\right], \tag{A.11}$$

View Article Online
DOI: 10.1039/C9SM02385B

where again to simplify the expression we defined

$$B(\kappa) = \sqrt{1-\kappa^2}\sqrt{1+(A^2-1)\kappa^2} + \frac{A^2}{\sqrt{A^2-1}} \arcsin \frac{\sqrt{1-\kappa^2}\sqrt{A^2-1}}{A^2}. \quad (A.12)$$

The external force applied to the particles is given by the derivative of the free energy with respect to distance $2r$ between them,

$$F = \frac{d\mathcal{F}}{d(2r)}, \quad (A.13)$$

We express free energy, volume and droplet profile as functions of the independent parameter κ defined by Eq (A.9). Then the force can be expressed as a function of κ by formula

$$F(\kappa) = \frac{1}{2}\frac{(d\mathcal{F}/d\kappa)}{(dr/d\kappa)}. \quad (A.14)$$

In order to calculate the derivatives in Equation (A.14), we need to express the free energy $\mathcal{F}$ and particle position r as functions of κ in small ν limit. We define dimensionless quantities

$$\lambda \equiv \frac{\rho_0 - R}{a} \quad (A.15)$$

and

$$\mu \equiv \frac{c}{\nu}, \quad (A.16)$$

and express them as functions of κ.

The actual contact angle at the surface of the particles in the absence of line tension is equal to contact angle at flat surface, θ. To express μ in terms of κ, we will henthforth use this result and fix the actual contact angle equal to θ expressed as

$$\theta = \arctan \frac{A\kappa}{\sqrt{1-\kappa^2}} - \arctan z'(\rho_c). \quad (A.17)$$

Substituting Eq. (A.5) and taking the limit $\nu \to 0$ we obtain Eq. (5).

To express λ in terms of κ we expand the volume given by Eq. (A.6) in powers of ν. Using the expansions of the elliptic integrals [37]

$$F(\varphi_c, k) = -\ln\frac{(\kappa+\xi)\nu}{4} + o(\nu^0) \quad (A.18)$$

and

$$E(\varphi_c, k) = 1 - \left\{\frac{\kappa^2}{2} + \frac{\mu^2}{16}\left[2\ln\frac{(\kappa+\xi)\nu}{4} - \frac{\kappa-\xi}{\kappa+\xi}\right]\right\}\nu^2 + o(\nu^2), \quad (A.19)$$

we obtain an approximate equation for the volume of the droplet

$$V = \frac{4\pi R^3}{3}\left[1 + 3\left(\lambda - \frac{\mu}{4}\right)\nu + \frac{3}{16}\left(16\lambda^2 - 12\lambda\nu - \mu^2\right)\nu^2 + o\left(\nu^2\right)\right]. \quad (A.20)$$

Requiring the volume of incompressible fluid in the droplet, given by equation (A.20), to be constant we can express λ in terms of κ as a series in ν:

$$\lambda = \frac{\mu}{4} + \frac{3\mu^2}{16}\nu + o(\nu^1). \quad (A.21)$$

Note that the assumption of incompressibility of inner fluid is also valid in the case of gaseous (e.g. air) bubbles, as discussed in Ref. [37].

Using the above expressions, we can write the free energy of the system in the following approximate form, valid for small $\nu = a/R$:

$$\mathcal{F}(\kappa) = \mathcal{F}_0 - 2\pi a^2\gamma\left\{\kappa^2 + \frac{\mu^2}{4}\left[\frac{\xi}{\kappa+\xi} + \ln\frac{(\kappa+\xi)\nu}{4}\right] + B(\kappa)\cos\theta\right\} + o(\nu^o), \quad (A.22)$$

where

$$\mathcal{F}_0 = 4\pi R^2\gamma \quad (A.23)$$

is free energy of undeformed droplet without adsorbed particles, and ξ is defined by Eq. (4).

In order to calculate force using Eq. (A.14), we also need the expression for the position of the particles, r, as a function of the parameter κ, too. Expressing the position of the particles as a sum of the r coordinate of the contact line and the displacement of particle centre with respect to contact line,

$$r = z(\rho_c) + A\sqrt{a^2 - \rho_c^2}, \quad (A.24)$$

and expanding in ν the function $z(\rho_c)$ given by Eq. (A.1), we obtain

$$r(\kappa) = R + a\left\{A\sqrt{1-\kappa^2} - \frac{\mu}{4}\left[1 + 2\ln\frac{(\kappa+\xi)\nu}{4}\right]\right\} + o(\nu^0), \quad (A.25)$$

which is equivalent to Eq. (3). Substituting Eqs (A.22) and (A.25) into Eq. (A.14), we finally obtain formula (2) for the force.

View Article Online
DOI: 10.1039/C9SM02385B 8

[1] J. C. Loudet, A. M. Alsayed, J. Zhang and A. G. Yodh, Phys. Rev. Lett., 2005, **94**, 018301.
[2] H. Lehle, E. Noruzifar and M. Oettel, Eur. Phys. J. E, 2008, **26**, 151–160.
[3] M. Oettel and S. Dietrich, Langmuir, 2008, **24**, 1425–1441.
[4] J. Guzowski, M. Tasinkevych and S. Dietrich, Phys. Rev. E, 2011, **84**, 031401.
[5] L. Botto, E. P. Lewandowski, M. Cavallaro and K. J. Stebe, Soft Matter, 2012, **8**, 9957–9971.
[6] G. B. Davies and L. Botto, Soft Matter, 2015, **11**, 7969–7976.
[7] P. Galatola, Phys. Rev. E, 2016, **93**, 022604.
[8] B. J. Newton, R. Mohammed, G. B. Davies, L. Botto and D. M. A. Buzza, ACS Omega, 2018, **3**, 14962–14972.
[9] J. H. Lim, J. Y. Kim, D. W. Kang, K. H. Choi, S. J. Lee, S. H. Im and B. J. Park, Langmuir, 2018, **34**, 384–394.
[10] A. M. Luo, J. Vermant, P. Ilg, Z. Zhang and L. M. Sagis, J. Coll. Int. Sci., 2019, **534**, 205–214.
[11] E. Noruzifar and M. Oettel, Phys. Rev. E, 2009, **79**, 051401.
[12] J. C. Loudet and B. Pouligny, EPL, 2009, **85**, 28003.
[13] J. C. Loudet and B. Pouligny, EPL, 2011, **34**, 76.
[14] B. Madivala, J. Fransaer and J. Vermant, Langmuir, 2009, **25**, 2718–2728.
[15] S. Dasgupta, M. Katava, M. Faraj, T. Auth and G. Gompper, Langmuir, 2014, **30**, 11873–11882.
[16] G. B. Davies, T. Krüger, P. V. Coveney, J. Harting and F. Bresme, Adv. Mater., 2014, **26**, 6715–6719.
[17] B. Madivala, S. Vandebril, J. Fransaer and J. Vermant, Soft Matter, 2009, **5**, 1717–1727.
[18] V. R. Dugyala, S. V. Daware and M. G. Basavaraj, Soft Matter, 2013, **9**, 6711–6725.
[19] G. Boniello, A. Stocco, M. Gross, M. In, C. Blanc and M. Nobili, Phys. Rev. E, 2016, **94**, 012602.
[20] S. Coertjens, P. Moldenaers, J. Vermant and L. Isa, Langmuir, 2014, **30**, 4289–4300.
[21] P. J. Yunker, T. Still, M. A. Lohr and A. G. Yodh, Nature, 2011, **476**, 308–311.
[22] J. Vermant, Nature, 2011, **476**, 286–287.
[23] X.-C. Luu and A. Striolo, J. Phys. Chem. B, 2014, **118**, 13737–13743.
[24] D. W. Kang, W. Ko, B. Lee and B. J. Park, Materials, 2016, **9**, 664.
[25] J. Faraudo and F. Bresme, J. Chem. Phys., 2003, **118**, 6518.
[26] F. Bresme and J. Faraudo, J. Phys. Cond. Mat., 2007, **19**, 375110.
[27] G. B. Davies, T. Krüger, P. V. Coveney, J. Harting and F. Bresme, Soft Matter, 2014, **10**, 6742–6748.
[28] M. G. Basavaraj, G. G. Fuller, J. Fransaer and J. Vermant, Langmuir, 2006, **22**, 6605–6612.
[29] J. de Graaf, M. Dijkstra and R. van Roij, J. Chem. Phys., 2010, **132**, 164902.
[30] F. Günther, S. Frijtersa and J. Harting, Soft Matter, 2014, **10**, 4977–4989.
[31] S. Coertjens, R. D. Dier, P. Moldenaers, L. Isa and J. Vermant, Langmuir, 2017, **33**, 2689–2697.
[32] B. Gabriel and J. Teissié, Proc. Natl. Acad. Sci. USA, 1996, **93**, 14521–14525.
[33] J. Drelich, Coll. Surf. A, 1996, **116**, 43–54.
[34] A. Amirfazli and A. W. Neumann, Adv. Coll. Int. Sci., 2004, **110**, 121–141.
[35] B. M. Law, S. P. McBride, J. Y. Wang, H. S. Wi, G. Paneru, S. Betelu, B. Ushijima, Y. Takata, B. Flanders, F. Bresme, H. Matsubar, T. Takiue and M. Aratono, Prog. Surf. Sci., 2017, **92**, 1–39.
[36] G. B. Davies, T. Krüger, P. V. Coveney and J. Harting, J. Chem. Phys., 2014, **141**, 154902.
[37] R. Ettelaie and S. V. Lishchuk, Soft Matter, 2015, **11**, 4251–4265.
[38] S. V. Lishchuk and R. Ettelaie, Langmuir, 2016, **32**, 13040–13045.
[39] J. Ally, M. Kappl, H.-J. Butt and A. Amirfazli, Langmuir, 2010, **26**, 18135–18143.
[40] O. Pitois and X. Chateau, Langmuir, 2002, **18**, 9751–9756.
[41] A. Sinha, A. K. Mollah, Hardt and R. Ganguly, Soft Matter, 2013, **9**, 5438–5447.
[42] C. Pozrikidis, Langmuir, 2007, **575**, 333–357.
[43] V. Poulichet and V. Garbin, Langmuir, 2015, **31**, 12035–12042.
[44] A. Maestro, E. Guzmán, F. Ortega and R. G. Rubio, Cur. Op. Col. Int. Sci., 2014, **19**, 355–367.
[45] J. Reguera, E. Ponomarev, T. Geue, F. Stellacci, F. Bresme and M. Moglianetti, Nanoscale, 2015, **7**, 5665–5673.
[46] F. Bresme and M. Oettel, J. Phys. Cond. Mat., 2007, **19**, 413101.
[47] W. Helfrich, Z. Naturforsch., 1973, **28c**, 693–703.

View Article Online
DOI: 10.1039/C9SM02385B

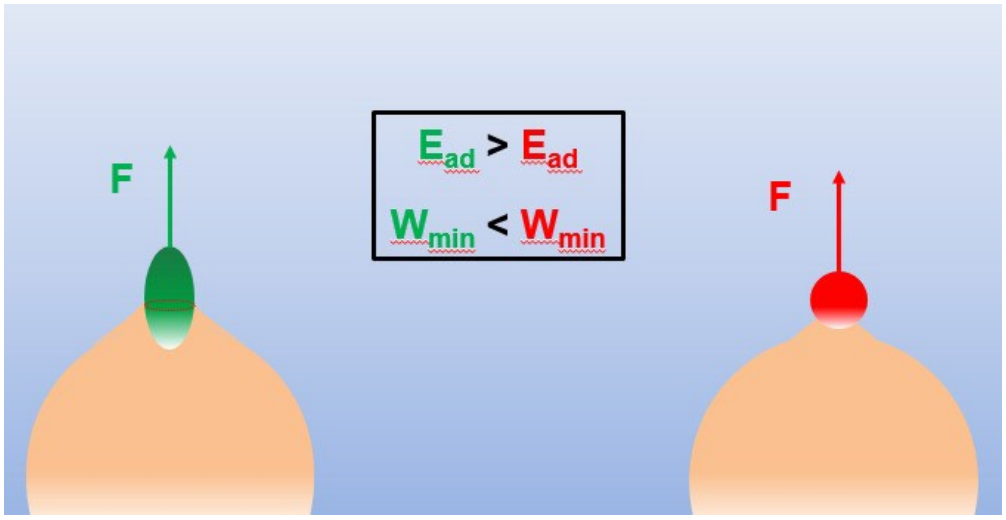

178x91mm (96 x 96 DPI)